Accepted for publication in the Journal of Wind Engineering and Industrial Aerodynamics, 10 Feb. 2023

Impact of a nearby car on the drag of a cyclist

Bert Blocken[*1,2], Stefanie Gillmeier[3], Fabio Malizia[2], Thijs van Druenen[3]

[1] *Anemos BV Company, Spechtendreef 3, 2460 Kasterlee, Belgium*
[2] *Building Physics and Sustainable Design, Department of Civil Engineering, KU Leuven, Kasteelpark Arenberg 40 - bus 2447, 3001 Leuven, Belgium*
[3] *Building Physics and Services, Department of the Built Environment, Eindhoven University of Technology, P.O. box 513, 5600 MB Eindhoven, the Netherlands*

**Corresponding author: Bert Blocken; bert.blocken@kuleuven.be; https://orcid.org/0000-0003-2935-9562*

Abstract
Cycling races contain a multitude of cars including team cars. During parts of the race, the cyclists can ride in close proximity of these cars. An earlier study indicated that there is a drag reduction for a cyclist by a following car. However, to the best of our knowledge, there is no information in the scientific literature about the impact of a car on cyclist drag when the cyclist is positioned either in-line behind the car or in parallel or staggered position with the car. This paper presents wind tunnel measurements and CFD simulations of cyclist drag for 29 different cyclist-car arrangements. It is shown that drafting in-line behind a car at a distance of 10 and 40 m leads to substantial drag reductions of about 20 and 7%, respectively. The staggered positions can lead to either a large drag increase up to almost 9% or a moderate drag decrease up to 1.4%. These drag changes can induce time gains or losses that go up to several seconds per kilometre, which is large enough to potentially influence the outcome of cycling races.

Keywords
Computational fluid dynamics; wind tunnel; aerodynamic cyclist drag; cycling aerodynamics, car

1. Introduction

At racing speeds above 40 km/h and on level terrain, the aerodynamic resistance or drag of a cyclist constitutes more than 90% of the total resistance (Kyle and Burke 1984; Grappe et al. 1997; Lukes et al. 2005). The other components of the total resistance are the rolling, wheel-bearing and drive-train resistance. Cycling aerodynamics research in the past decades has mainly focused on the aerodynamics of bicycles, isolated cyclists and cyclist groups, as documented in some recent review papers (Crouch et al. 2017; Malizia and Blocken 2020; 2021).

In a cycling race, several cars and motorcycles are present and during parts of the race the cyclists can ride in close proximity of these cars or motorcycles. In such cases, these in-race motorised vehicles can influence the drag of the cyclist, which might lead to unfair aerodynamic advantages or disadvantages. A number of previous studies assessed the aerodynamic impact of nearby cars and motorcycles. Blocken and Toparlar (2015) demonstrated that a team car following a cyclist can provide an aerodynamic benefit to this cyclist due to the so-called subsonic upstream disturbance. This refers to the fact that below the speed of sound, the governing Navier-Stokes differential equations exhibit elliptical behaviour, which implies that every object moving in a fluid not only disturbs the flow downstream of it, but also in front of it and next to it. Based on CFD simulations validated with wind tunnel tests, it was shown that a car riding at distances of 3, 5 and 10 m behind a cyclist can yield cyclist drag reductions of 3.7, 1.4 and 0.2%, respectively. Later, Blocken et al. (2016) demonstrated the same effect for a motorcycle following a cyclist, yielding drag reductions for the cyclist of 3.8, 0.3 and 0.1% for separation distances of 1, 5 and 10 m, respectively.

While the beneficial effect for a cyclist by a following vehicle might be perceived as counter-intuitive, it is well-known that a cyclist riding behind a vehicle can obtain large drag reductions. This was already known shortly after the invention of the safety bicycle as illustrated by drafting races held at the end of the 19th century, where cyclists attempted top speeds by drafting behind a multi-rider tandem, a motorcycle with a wind screen or even a train (Fig. 1 as reported by Malizia and Blocken 2021). A situation that occurs quite often in road races, albeit generally either for a short period of time (e.g. few seconds) or at a fairly large separation distance (e.g. 20 or 30 m), is that in which a cyclist is drafting behind a motorcycle. While it is well-known that this can yield large benefits, it was not known how large these benefits can be. Applying wind tunnel tests and CFD simulations, Blocken et al. (2020) demonstrated that drafting at 2.64, 10, 30 and 50 m behind a motorcycle could yield drag reductions of 48, 23, 12 and 7%, respectively. However, to the best knowledge of the authors, such a study does not yet exist for a cyclist drafting behind a car. Such situations also occur quite frequently in road

races, as shown in Fig. 2a,b. They might give cyclists substantial benefits, as a car is a large object that could substantially shield the cyclist from the wind and significantly reduce its drag, which allows either saving energy or riding faster, or both. Because cycling races are sometimes decided based on seconds or less, or on centimetres, this undesired drafting effect could potentially affect the outcome of the race. Analysing the drag reductions for a cyclist by drafting behind a car is the first objective of the present paper.

Apart from riding in front or behind a motorcycle, it can also happen that the cyclist is riding side-by-side to a motorcycle or in staggered position with respect to this motorcycle. Camera and photographer motorcycles for example can ride next to a cyclist for a while to gather nearby video footage and photos. A recent study showed that riding side-by-side at a lateral distance of 1 to 2 m can lead to a 10 to 5% drag increase, respectively, for the cyclist and that a staggered arrangement can lead to either a drag increase or a drag decrease, where the latter goes up to about 2% for most positions analysed (Blocken et al. 2021). Also team cars can ride next to a cyclist for communication between coach and rider (Fig. 2c-e) or for handing over drinking bottles to the rider (Fig. 2f). During the latter action, sometimes the cyclist receives some momentum from the car by holding the bottle for a short period of time while it is also being held by the coach in the car, as shown in Fig. 2f, i.e. the so-called "sticky bottle". Outside the short time period of the "sticky bottle", the presence of the car will influence the drag of the cyclist. Also here, this could affect the energy consumption and/or cycling speed, which could potentially affect the outcome of the race. However, to the best knowledge of the authors, studies on the aerodynamic impact of a cyclist parallel to a car or in staggered position to a car have not yet been published. Such an analysis is the second objective of the present paper.

Outside the scope of the present paper, only Blocken and Toparlar (2015) and Gromke and Ruck (2021) analysed the aerodynamic interaction between a cyclist and a car. The latter authors performed field tests to assess the lateral loads on cyclist dummies by an overtaking station wagon. In the present paper however, only the longitudinal air resistance (i.e. in the riding direction) is studied.

The present paper presents wind tunnel tests and CFD simulations to assess the aerodynamic benefit for a cyclist drafting in-line behind a car and the aerodynamic impact on a cyclist by a nearby car in parallel and staggered position. The CFD simulations are also exploited to explain the reasons for the observed aerodynamic impacts. A power model is used to convert the drag changes to potential time savings or losses for the cyclist.

2. Wind tunnel set-up

The wind tunnel (WT) tests were performed at quarter scale. The WT models are shown in Figure 3 and 4. Figure 3 indicates their equivalent full-scale dimensions. The cyclist model geometry was obtained by 3D scanning with an Artec Eva scanner. It represents a male cyclist with a height of 183 cm and body mass of 72 kg in a time-trial position. The scan was postprocessed in order to make the athlete unrecognisable. The procedure of obtaining written consent from the cyclist, scanning, processing the body geometry and reporting the results was approved by the ethical review board of Eindhoven University of Technology with reference code (ERB2020BE_1859456_WT). The bicycle was a standard race bicycle with tri-spoke front wheel, disk rear wheel and a time-trial handlebar. Details such as gears, chain and cables were not withheld in the model geometry. The full-scale frontal area of cyclist and bicycle was 0.34 m^2. To ensure sufficient model strength and stiffness, vertical reinforcement bars were added to the cycling wheels and the bicycle was fixed on a small model bottom plate (see Fig. 4). The cyclist model was manufactured by CNC milling. The car model was obtained from an online data base of estate wagons. Surface details were removed or smoothened except for the rear-view mirrors. While team cars – as opposed to commissaire and other cars – generally carry bicycles and separate wheels on their roof, these items were not included in this study. The car model had a full-scale frontal area of 2.33 m² and was manufactured by 3D printing.

The tests were performed in the WT of Eindhoven University of Technology. Figure 4a shows a photo with the cyclist model in-line behind the car model and Figure 4b-d show photos with the cyclist model at different positions next to the car model. Figures 4 and 5 show the WT set-up in the test section with the cyclist and car positioned on a sharp-edged elevated plate with embedded force sensor. The plate consists of a wooden plate covered by a thin metal plate. Note that the holes in the metal plate are not present in the wooden plate below it. The maximum blockage ratio of the set-up was below the recommended maximum of 5% for WT tests (ASCE 1999). The elevated plate was used to limit the boundary layer height on the plate. The cyclist model was placed on the force sensor. The force sensor was designed and manufactured in house specifically for high-accuracy quarter-scale cyclist WT tests (Blocken et al. 2018) with an accuracy of 0.001 N. The measured longitudinal turbulence intensity at the model position was 0.3%. Data were sampled at 10 Hz for 60 s. Tests were performed at wind speeds of 15, 20, 25 and 30 m/s in order to detect Reynolds number independence, which was noted above 20 m/s. The Reynolds number independent results were retained and are reported in the remainder of this paper. It was assumed that there was no crosswind, no head wind and no tail wind, therefore the WT speed represented the riding velocity of cyclist and car.

Three different sets of WT tests were performed. All distances below are reported in full-scale values. The first set focused on the cyclist drafting behind the car and included ten separation distances (i.e. the distance between rear of car and the front wheel of cyclist) ranging from 0.06 m to 19.2 m. The second set focused on the staggered arrangements of cyclist and car with a fixed lateral distance and 14 different streamwise positions of the cyclist with respect to the car. The third set focused on the parallel arrangements of cyclist and car with fixed streamwise position but four different lateral distances. To assess the repeatability of the experimentally obtained drag values, the drag of the isolated cyclist was measured five times by detaching and remounting the model on the force sensor. The resulting repeatability of the obtained drag values was found to be 0.7-0.9%, which corresponded to drag differences of about 0.3 N for the isolated cyclist. All drag measurements were corrected to match the following reference values: 101325 Pa (standard atmosphere), 15°C, 15 m/s (a top time trial speed) and full geometrical scale.

3. CFD simulation set-up

The CFD simulations were not performed at the WT scale but at the equivalent full scale. Because Reynolds number independence was observed in the WT at the reduced scale, it is considered justified to compare the results of the reduced-scale WT tests with those of the full-scale CFD simulations. The computational geometries of the cyclist and car were identical to those of the WT models apart from the model bottom plate below the WT bicycle, the vertical reinforcement bars in the bicycle wheels and the geometrical scale (1:1 versus 1:4). The rectangular computational domains had dimensions length x width x height ranging from 60 x 32 x 24 m³ up to 100 x 32 x 24 m³. The maximum blockage ratio was about 0.5%, which is below the recommended maximum of 3% for CFD simulations (Franke et al. 2007; Tominaga et al. 2008; Blocken 2015).

The computational domains were discretised with hybrid hexahedral-tetrahedral grids based on both general grid generation guidelines (Casey and Wintergerste 2000; Tucker and Mosquera 2001; Franke et al. 2004; 2007; Tominaga et al. 2008; Blocken 2015) and grid generation guidelines developed specifically for cyclist aerodynamics simulations (Blocken et al. 2013; Mannion et al. 2018; Malizia et al. 2019; Malizia and Blocken 2020). To accurately resolve the thin boundary layer including the laminar sublayer, the wall-adjacent cell size was 20 micrometre (= 0.02 mm) and 40 layers of prismatic cells were applied near the cyclist and car surfaces (Fig. 6). The resulting dimensionless wall unit y* had values that were generally below 1 and everywhere below 5. The cell size in the area between cyclist and car was at most 0.03 m. The total cell count ranged from 38.3×10^6 to 60.3×10^6.

Wheel rotation was not modelled, neither for the cyclist, nor for the car. At the inlet, a uniform velocity of 15 m/s was imposed that represented the riding velocity. The inlet turbulence intensity was set to 0.5% to obtain the same approach-flow value of 0.3% in the region directly upstream of the car as in the WT tests. This was required because the turbulence intensity decayed from 0.5 to 0.3% from the inlet of the computational domain to the position of the car model. At the outlet, zero static gauge pressure was set. The bottom, side and top surfaces of the domain were slip walls. The surfaces of the cyclist and car were no-slip walls, where the cyclist body had a surface roughness with equivalent sand-grain roughness height $k_S = 0.1$ mm and the bicycle and car had $k_S = 0$ mm.

The earlier study of a cyclist drafting behind a motorcycle by Blocken et al. (2020) illustrated that 3D Reynolds-averaged Navier-Stokes (RANS) simulations with the Shear Stress Transport (SST) k–ω model (Menter 1994) with curvature correction in pseudo-transient formulation could accurately reproduce the drag reduction only for very short separation distances up to 4.8 m while for larger distances deviations ranging from 30% for 10 m distance to 60% for 50 m distance were obtained, due to inaccurate reproduction of the von Karman vortex shedding in the far wake. Therefore, similarly to the study by Blocken et al. (2020) for the larger distances, also in the present paper, Scale Adaptive Simulations (SAS) (Menter and Egorov 2010) were performed involving the Shear Stress Transport (SST) k-ω model with curvature correction. Pressure-velocity coupling was performed by the PISO algorithm. Pressure interpolation was second order, gradient interpolation was conducted with the Green-Gauss node based scheme. Bounded central differencing was used for the momentum equations and second-order discretisation for the turbulence model equations. Time discretisation was bounded second order implicit. The simulations were performed with the commercial CFD code Ansys Fluent 16.1 (2015). The time step of 0.002 s was selected such that the CFL number was equal to unity or below unity in the area between the cyclist and the car, both in streamwise and in lateral direction. This time step also resulted from a time step convergence analysis as reported in (Blocken et al. 2020). After an initialisation period of 1500 time steps, the number of additional or sampling time steps required to obtain a constant moving average of the sampled drag values ranged from about 4000 to 28000. The averaged drag values over this number of sampling time steps are the values reported in the next section.

4. Results

4.1. Cyclist drafting in-line behind car

Figure 7 presents the results of the WT measurements and SAS CFD simulations for the cyclist drafting in-line behind the car in terms of drag reduction compared to a cyclist riding alone. Due to the limited length of the sharp-edged elevated plate in the WT, the measurements were only made up to an equivalent full-scale distance of 19.2 m. After the WT measurements, first, the CFD simulations at 5.28, 10.56, 14.40 and 19.20 m were performed, for two reasons: (1) to allow validation based on the WT measurements that were also conducted for these distances; (2) to provide the typical CFD whole-flow field data of mean and instantaneous velocity and static pressure to explain the reasons behind the obtained drag reductions. Next, after validation for these shorter distances, the CFD simulations were applied to obtain the cyclist drag reduction for distances of 30 and 40 m, which were not obtained by the WT measurements.

The comparison of the WT and CFD results shows a fairly good agreement. The maximum drag reduction for the cyclist was almost 80% for the very short distance of 0.06 m, but also for 0.96 m the reduction was still very large and equal to about 75%. At about 10 m distance, the drag reduction was about 20% while it decreased to about 7% for a distance of 40 m. The latter number illustrates that the far wake behind a team car is a persistent phenomenon that even at very large distances can still provide a substantial benefit.

Figure 8 depicts contours of the instantaneous and mean velocity ratio K and pressure coefficient C_P in a horizontal plane at 1 m height and in a vertical centre plane for a separation distance of 10 m. K is defined as the ratio of the local wind speed and the riding velocity of 15 m/s. C_P is defined as the local static pressure divided by the dynamic pressure associated with the riding velocity. Figure 8a illustrates the vortex shedding in the near and far wake behind the car and the position of the cyclist in this far wake. The cyclist is clearly exposed to a much lower velocity than the riding velocity. Figures 8b,d suggest that this velocity is about 88-90% of the riding velocity. which roughly corresponds to the obtained drag reduction of about 20%. Figures 8c,d show that the far wake behind the car keeps expanding in the vertical direction with increasing distance downstream, while the opposite seems to occur in the horizontal plane (see Fig. 8b). Figures 8e and g illustrate the alternation of high and low static pressure regions shed from the car and approaching the cyclist while Figures 8f and h show the mean pressure fields around car and cyclist but these are less elucidating in terms of the cyclist drag reduction.

Figure 9 illustrates contours of the instantaneous and mean velocity ratio K in the same two planes as before, for a separation distance of 40 m. They clearly show the existence and persistence of the far wake with vortex shedding behind the car down to at least 40 m downstream distance. The cyclist seems to be present in a region with K of about 0.96, which roughly corresponds with a drag reduction of 7%. Figure 9c and d show the continuing vertical expansion of the wake with increasing downstream distance.

Figure 10 displays contours of the instantaneous and mean C_P in the same two planes for a separation distance of 40 m. These images do not show a clear presence of high and low static pressure areas close to the cyclist, given the large separation distance.

4.2. Cyclist in staggered position with respect to car

Figure 11 holds the results of the WT measurements and SAS CFD simulations for the cyclist in staggered position with respect to the car, with lateral distance $\Delta y = 1.5$ m. Here, the CFD simulations were only made to provide the typical CFD whole-flow field data of velocity and static pressure to aid in explaining the reason behind the drag changes. The agreement between the WT and CFD results is moderate. The deviation is rather large for the situation with the cyclist at 3.84 m downstream of the nose of the car, while the agreement for the other two positions is fair. It is not clear what has contributed to these differences, although the presence of the vertical reinforcement bars in the wheels of the cyclist model and the bottom plate might have had an influence here as the flow near the cyclist will have had a more pronounced lateral component.

Substantial drag increases were observed when the cyclist was riding next to the car. When the front wheel and nose of the car were aligned in streamwise direction, the WT measured drag increase was 7%. This increased towards 8.2% when the cyclist was positioned at 1.92 m downstream of the nose of the car. Small drag increases were still present when Δx_2 was 4.8 m (cyclist positioned downstream of nose of car) or -1.92 m (cyclist positioned upstream of nose of car). For larger distances downstream or upstream, there was a small drag benefit for the cyclist. For the downstream positions, this benefit increased as the cyclist position moved further downstream and became more thoroughly positioned in the wake of the car. The benefit reached 1.3% for $\Delta x_2 =$ 7.68 m. For the upstream positions, the benefit was attributed to the fact that the position of the cyclist was sufficiently upstream of the car to benefit from the subsonic upstream disturbance (Blocken et al. 2013, Blocken and Toparlar 2015). The subsonic upstream disturbance yielded a maximum benefit of about 0.5% at $\Delta x_2 =$ -3.84 m but decreased further upstream. Indeed, it is known from previous studies that the subsonic upstream

disturbance benefit rapidly fades out with increasing upstream distance (Blocken et al. 2013; 2016; Blocken and Toparlar 2015).

Figure 12 shows the results for different lateral distances Δy when the front wheel of the bicycle and the nose of the car were aligned in the streamwise direction. It shows an almost linear decrease of the percentage of drag increase with increasing Δy, suggesting that the drag increase would only reduce to zero near Δy = 6 m, which is a distance often impossible to attain on cycling roads given their limited widths and given the width of the car.

Figure 13 depicts contours of instantaneous and mean K and C_P in a horizontal plane at 1 m height for the cyclist next to the car with $\Delta x_2 = 0$ and Δy = 1.5 m. Figure 13a and b show areas of increased wind speed at the sides of the car, with the cyclist located in part of these areas but not completely. Therefore, the cyclist experienced a larger wind speed, which increased its resistance. Figures 13c,d illustrate that the rear of the cyclist connected with the low-pressure area at the side of the car, which increased the cyclist drag. Figure 14 shows contours of instantaneous and mean K and C_P in horizontal plane at 1 m height for cyclist next to car with $\Delta x_2 = 2$ m and Δy = 1.5 m. Also here the cyclist was clearly positioned in an area with higher wind speed but to a larger degree as for $\Delta x_2 = 0$, so the drag increase was more pronounced. Also the merging with the low-pressure area next to the car was more pronounced. Figure 15 shows the same type of contours but here the cyclist was positioned further downstream so slightly outside the area of largest wind speed increase at the sides of the car, and also a bit further downstream of the main underpressure area besides the car. This led to a lesser drag increase as for $\Delta x_2 = 2$ m.

4.3. Drafting behind car versus behind motorcycle

Figure 16 compares the drag reduction percentages for a cyclist drafting in-line behind a car versus drafting in-line behind a motorcycle, where the latter data is taken from (Blocken et al. 2020). It clearly shows that nearby drafting behind a car is more beneficial than behind a motorcycle, up to a separation distance of about 5 to 7 m. Beyond that distance, drafting behind a motorcycle is more beneficial. The reason is the geometry of the wake behind these vehicles. Because the car is a larger body than the motorcycle, the near wake of the car has lower velocities than behind the motorcycle. This leads to a slightly larger benefit for the cyclist. However, because the motorcycle is higher than the car (1.906 versus 1.456 m), at larger distances, the vertical velocity deficit over the height of the cyclist (1.554 m) is more pronounced behind the motorcycle than behind the car, at least if the cyclist is perfectly in-line with the motorcycle and car. A motorcycle with two persons sitting upright is also a less aerodynamic object than the car. This leads to a larger benefit for the cyclist behind the motorcycle in the far wake.

4.4. Potential time gains and losses

Martin et al. (1998) developed a comprehensive road cycling power model that was employed here to convert the drag change percentages as shown in Figures 7, 11 and 12 to potential speed changes and potential time gains or losses:

$$P_{tot} = (P_{ad} + P_{rr} + P_{wb} + P_{pe} + P_{ke})(\frac{1}{\eta}) \quad (1)$$

With P_{tot} the required power, P_{ad} the power loss due to aerodynamic drag, P_{rr} the power loss due to rolling resistance, P_{wb} the power loss due to friction in the wheel bearings, P_{pe} the power changes due to a change in potential energy and P_{ke} the power changes due to a change in kinetic energy. The efficiency η is that of the cyclist power transmission, associated with the friction in the drivetrain. For simplicity, we assumed level terrain and constant cycling speed so $P_{pe} = P_{ke} = 0$, and no crosswind, headwind or tailwind. Eq. (1) then becomes:

$$P_{tot} = [0.5\rho U^3(C_D A + F_w) + UC_{rr}mg + U(91 + 8.7U) \cdot 10^{-3}]\frac{1}{\eta} \quad (2)$$

The following parameter values were used: density ρ = 1.225 kg/m³, reference situation is a cyclist riding alone at U = 13 m/s, drag area $C_D A = 0.21$ m², wheel rotational drag area $F_w = 0.001$ m², rolling resistance coefficient $C_{rr} = 0.002$, cyclist-bicycle system mass m = 75 kg, gravitational constant g = 9.81 m/s² and chain efficiency η = 0.97698. These values led to $P_{tot} = 342$ W for the cyclist riding alone at 13 m/s. To relate drag changes to speed changes and time gains or losses, it was assumed that the cyclist kept providing the same power P_{tot} (= 342 W) when riding nearby the car. Table 1 presents the associated speed changes and the potential time gains or losses per km and per minute for the situation of the cyclist drafting behind the car for the separation distances in Figure 7. Table 2 presents the same for the cyclist parallel to the car or in staggered position. Because races are

sometimes won based on a few seconds or even tenths or hundreds of a second, it is clear that these unwanted and unfair time gains can be very large and can be decisive.

5. Limitations and discussion

The study has some limitations. It did not consider wheel rotation and pedalling although those aspects were not expected to impact the results significantly, as discussed in Blocken et al. (2018). The study only focused on one cyclist geometry and one position on the bicycle. The numbers of drag reduction, velocity change and time gains and losses provided should therefore be considered primarily as indicative. The study did also not consider cross wind, head wind or tail wind scenarios. For the situation of the cyclist drafting behind the car, when there is a cross wind, it will be more difficult or even impossible to benefit from the drafting effect, certainly for the larger distances. When there is a head wind (without cross wind component), the drafting benefit will be larger, while in case of a tail wind (without cross wind component), the drafting benefit will be smaller. Atmospheric turbulence, for example due to other cyclists or vehicles riding in front or next to the car, is expected to disturb the slipstream behind the car and could therefore somewhat mitigate the drafting benefit, although this should be clarified by future work.

This study only considered a cyclist riding at the same speed of the car. Future work can focus on cyclists approaching behind a car, or a car accelerating so the distance from the cyclist increases, or cars passing the cyclist at different speeds and lateral distances. Another interesting effect that could be studied is the impact of TV helicopters on cyclist drag, although contemporary helicopter TV recordings occur at much larger height and are more controlled than in the past.

The comparison of WT and CFD drag percentages revealed some significant differences that were at least partly attributed to the vertical reinforcement bars in the wheels of the WT model and the presence of the WT model bottom plate. In the future, a more sophisticated approach could involve a strength and stiffness analysis by combined CFD and finite element analysis (FEA) to minimise the size of the WT reinforcement bars and the bottom plate, with the aim to obtain a better final agreement between WT and CFD results.

The practical intention of this study is to inform the cycling world including cyclists, coaches, team managers but also the International Cycling Union (UCI) about the quantitative aerodynamic effects of riding in the vicinity of a car. Note that the earlier study on a cyclist riding in front of a car (Blocken and Toparlar 2015) has recently incited the UCI to actively engage with the first author and to adjust their regulations so as to increase the minimum distance for time trials between cyclist and car from 10 m to 25 m (Rogers 2022, UCI 2023). If carefully and strictly enforced, this rule change strongly contributes to both the fairness and safety of the races. It avoids the significant potential aerodynamic advantages when a car closely follows a rider and it allows a larger breaking distance – noting that no car of estate size has a breaking distance of 10 m even on a dry road. Similarly, it is hoped that the other publications by these authors on the aerodynamic impact of nearby in-race vehicles, including the present one, might be used in the future to improve the regulations in order to reduce undesired aerodynamic advantages. However, note that it is much easier to set regulations for a vehicle following a cyclist than for a vehicle riding in front of a cyclist, because in the former case, at relatively short minimum distances of 25 to 30 m, the aerodynamic impact becomes negligible, while in the latter case, much larger distances are required to avoid any significant aerodynamic benefit.

6. Summary and conclusions

Cycling races contain a multitude of cars including team cars. During parts of the race, the cyclists can ride in close proximity of these cars. An earlier study indicated the drag reduction for a cyclist by a following car. However, to the best of our knowledge, there was no information in the scientific literature about the impact of a car on cyclist drag when the cyclist is positioned either in-line behind the car or in parallel or staggered position with the car. This paper presented wind tunnel measurements and CFD simulations of cyclist drag for 29 different cyclist-car arrangements. It was shown that drafting in-line behind a car at a distance of 10 and 40 m leads to substantial drag reductions of about 20 and 7%, respectively. The staggered positions can lead to either a large drag increase up to almost 9% or a moderate drag decrease up to 1.4%. These drag changes can induce time gains or losses that go up to several seconds per kilometre, which is large enough to potentially influence the outcome of cycling races. Comparing the present results with a previous study of a cyclist drafting in-line behind a motorcycle, it was shown that nearby drafting behind a car is more beneficial than behind a motorcycle, up to a separation distance of about 5 to 7 m. Beyond that distance, drafting behind a motorcycle is more beneficial.

Acknowledgements

We thank the technical support team of the Wind Tunnel Laboratory at Eindhoven University of Technology: Ing. Jan Diepens, Geert-Jan Maas and Stan van Asten. This work was sponsored by SURF supercomputing in the Netherlands. The authors gratefully acknowledge the partnership with Ansys CFD. The authors also thank the two anonymous reviewers for their constructive and very valuable comments.

References

ANSYS Inc (2015) Ansys Fluent Theory Guide, Release 16.1, Canonsburg

ASCE (1999) Wind Tunnel Studies of Buildings and Structures, Aerospace Division of the American Society of Civil Engineers, 1999, ISBN 978-0-7844-0319-8.

Blocken B (2015) Computational Fluid Dynamics for urban physics: Importance, scales, possibilities, limitations and ten tips and tricks towards accurate and reliable simulations. Build Environ 91:219–245

Blocken B, Defraeye T, Koninckx E, Carmeliet J, Hespel P. 2013. CFD simulations of the aerodynamic drag of two drafting cyclists. Comput Fluids 71: 435-445.

Blocken B, Gillmeier S, Malizia F, van Druenen T (2021) Impact of a motorcycle on cyclist aerodynamic drag in parallel and staggered arrangements. Sports Engineering 24: Art. 7.

Blocken B, Malizia F, van Druenen T, Gillmeier SG (2020) Aerodynamic benefit for a cyclist by drafting behind a motorcycle. Sports Engineering 23: 19.

Blocken B, Toparlar Y (2015) A following car influences cyclist drag: CFD simulations and wind tunnel measurements. J Wind Eng Ind Aerodyn 145:178–186

Blocken B, Toparlar Y, Andrianne T (2016) Aerodynamic benefit for a cyclist by a following motorcycle. J Wind Eng Ind Aerodyn 155:1–10

Blocken B, van DruenenT, Toparlar Y, Malizia F, Mannion P, Andrianne T, Marchal T, Maas GJ, Diepens J, (2018) Aerodynamic drag in cycling pelotons: New insights by CFD simulation and wind tunnel testing. J Wind Eng Ind Aerodyn 179:319–337

Casey M, Wintergerste T (2000) Best Practice Guidelines. ERCOFTAC Special Interest Group on ‘‘Quality and Trust in Industrial CFD’’. ERCOFTAC

Crouch TN, Burton D, LaBry, ZA, Blair KB (2017) Riding against the wind: a review of competition cycling aerodynamics. Sport Eng 20:81–110

Franke J, Hellsten A, Schlünzen H, Carissimo B (2007) Best practice guideline for the CFD simulation of flows in the urban environment, COST action 732

Franke J, Hirsch C, Jensen AG, Krüs HW, Schatzmann M, Westbury PS, Miles SD, Wisse JA, Wright NG. 2004. Recommendations on the use of CFD in wind engineering. Proc. Int. Conf. Urban Wind Engineering and Building Aerodynamics, (Ed. van Beeck JPAJ), COST Action C14, Impact of Wind and Storm on City Life Built Environment, von Karman Institute, Sint-Genesius-Rode, Belgium, 5 - 7 May 2004.

Grappe F, Candau R, Belli A, Rouillon JD (1997) Aerodynamic drag in field cycling. Ergonomics 40:1299–1311

Gromke C, Ruck B (2021) Passenger car-induced lateral aerodynamic loads on cyclists during overtaking. J Wind Eng Ind Aerodyn 209: Art. 104489.

Gronen W, Lemke W (1987) Geschichte des Radsports. Fuchs-Druck und Verlag.

Kyle CR, Burke ER (1984) Improving the racing bicycle. Mech Eng 34–45

Lukes RA, Chin SB, Haake SJ (2005) The understanding and development of cycling aerodynamics. Sport Eng 8:59–74

Malizia F, Blocken B (2020) Bicycle aerodynamics: history, state of the art and future perspectives. J Wind Eng Ind Aerodyn 200:104134

Malizia F, Blocken B (2021) Cyclist aerodynamics through time: better, faster, stronger. J Wind Eng Ind Aerodyn 214: Art. 104673.

Malizia F, Montazeri H, Blocken B (2019) CFD simulations of spoked wheel aerodynamics in cycling: impact of computational parameters. J Wind Eng Ind Aerodyn 194: Art.nr. 103988.

Mannion P, Toparlar Y, Blocken B, Hajdukiewicz M, Andrianne T, Clifford E (2018). Improving CFD prediction of drag on Paralympic tandem athletes: influence of grid resolution and turbulence model. Sports Engineering 21(2):123-135.

Martin JC, Milliken DL, Cobb JE, McFadden KL, Coggan AR (1998) Validation of a mathematical model for road cycling. J Appl Biomech 14:276–291

Menter F, Egorov Y (2010) The scale-adaptive simulation method for unsteady turbulent flow predictions. Part 1: theory and model description. Flow Turb Combust 85:113–138

Menter FR (1994) Two-equation eddy-viscosity turbulence models for engineering applications. AIAA J 32(8):1598–1605

Rogers M (2022) Personal communication with Michael Rogers, Head of Road & Innovation, International Cycling Union (UCI)
UCI (2023) UCI regulations for road cycling: changes for time trials. International Cycling Union Press Release on 16 January 2023: https://www.uci.org/pressrelease/uci-regulations-for-road-cycling-changes-for-time-trials/1QmN4gRxrsgeQtgahAAfXr. Retrieved on 22 January 2023.
Tominaga Y, Mochida A, Yoshie R, Kataoka H, Nozu T, Yoshikawa M, Shirasawa T (2008) AIJ guidelines for practical applications of CFD to pedestrian wind environment around buildings. J Wind Eng Ind Aerodyn 96:1749–1761
Tucker P, Mosquera A (2001) NAFEMS introduction to grid and mesh generation for CFD. NAFEMS CFD Work. Group.

FIGURES AND TABLES

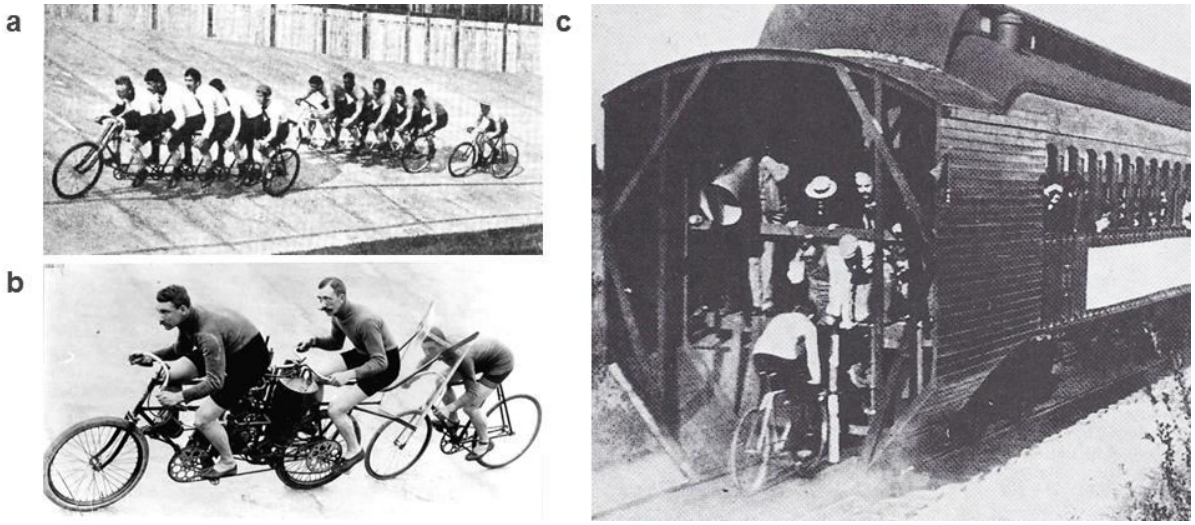

Fig. 1. (a) Cyclist drafting behind five-rider tandem in 1896; (b) Cyclist drafting behind a motorcycle equipped with a wind shield in 1894; (c) Cyclist drafting behind a train in 1899 (source: Gronen and Lemke, 1987).

Fig. 2. (a,b) Photos of a cyclist drafting behind a car in different race situations. Photos by (a) Luc Claessen; (b) Tim de Waele. (c-f) Photos of cyclist riding next to a car in different race situations. Photos by (c,d) Bas Czerwinski; (e) Stuart Franklin; (f) Bob Cullinan. (a-e) © Getty Images and (f) © Shutterstock, all reproduced with permission.

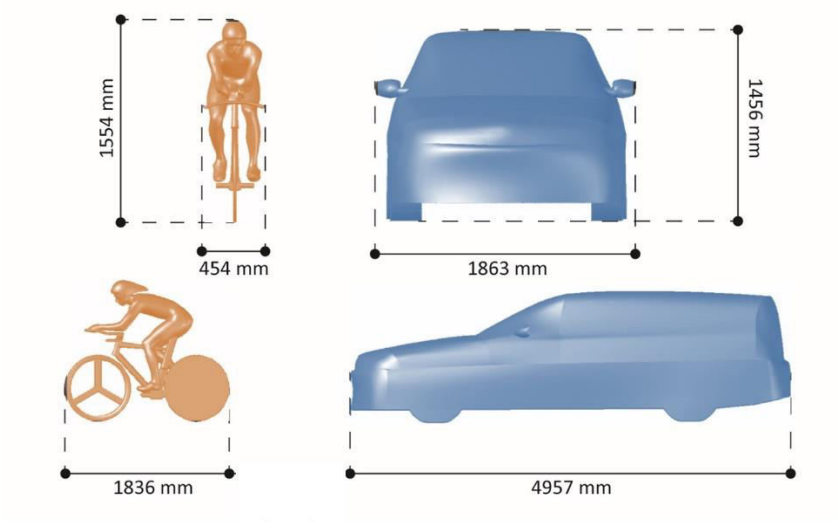

Fig. 3. Wind tunnel models of cyclist and car with indication of full-scale dimensions.

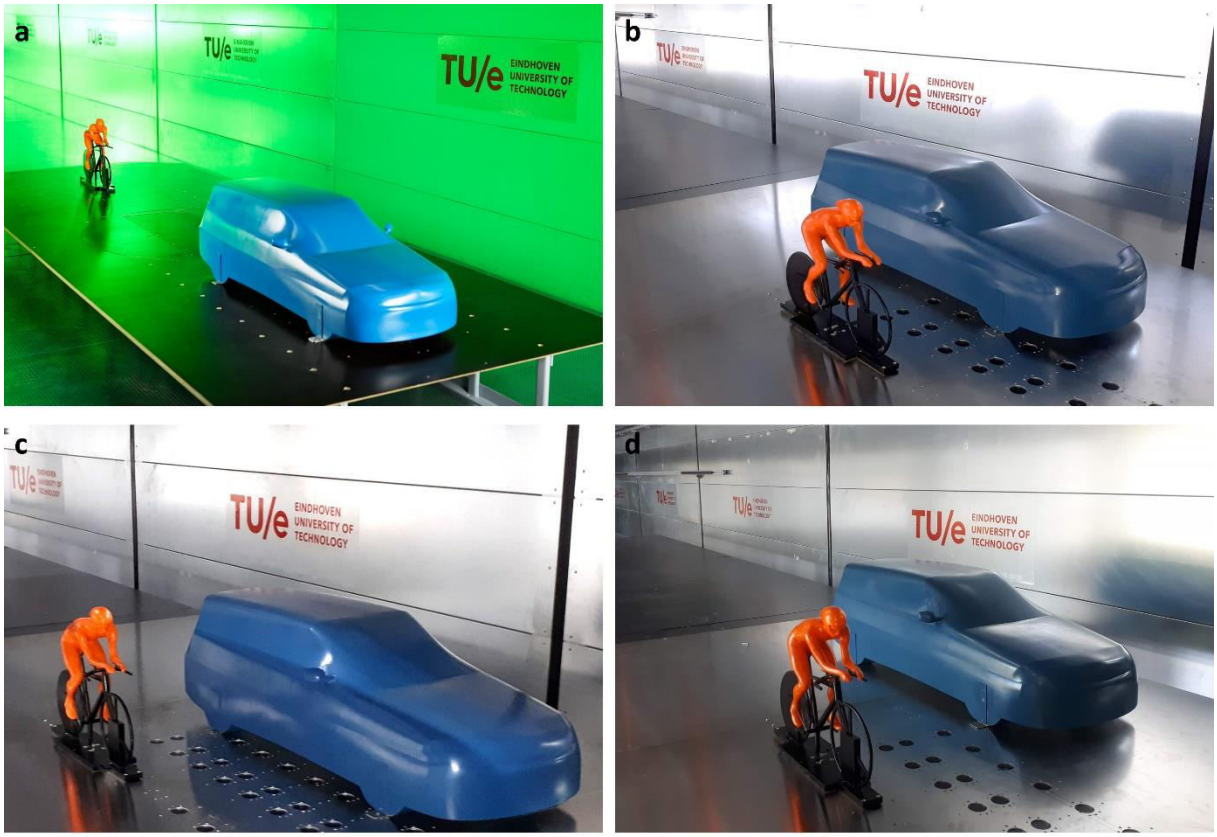

Fig. 4. Photos of wind tunnel models and wind tunnel set-up: (a) cyclist behind car and (b-d) cyclist next to car on elevated sharp-edged plate.

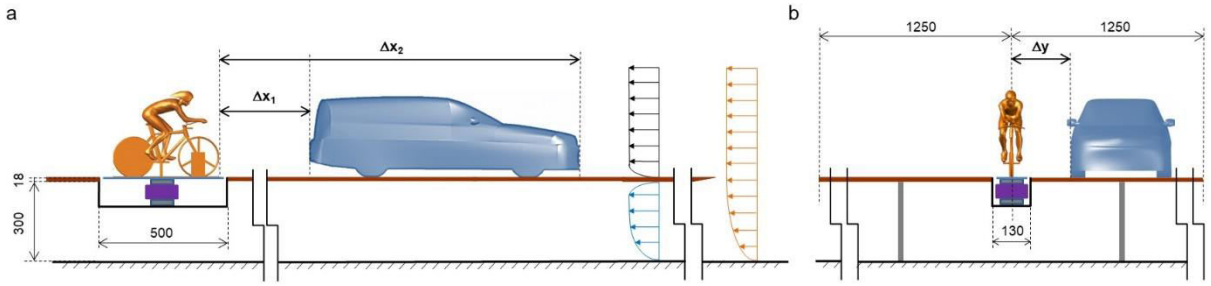

Fig. 5. Wind tunnel set-up: cyclist and car in staggered position on elevated sharp-edged plate: (a) Side view; (b) Front view. Dimensions in mm.

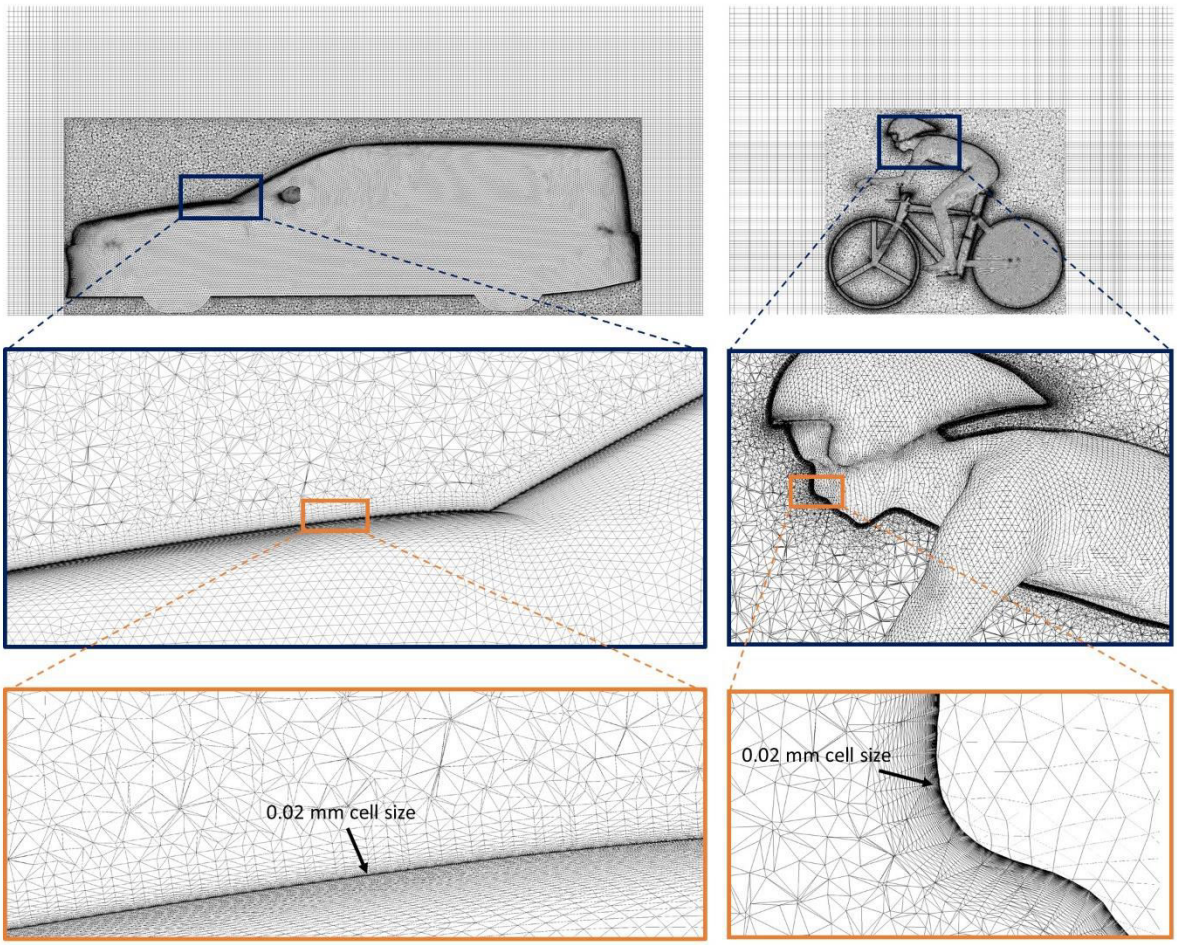

Fig. 6. Computational grid on cyclist and car surfaces and in vertical centre plane. Minimum cell size: 0.02 mm. Total cell count ranged from 38.3×10^6 to 60.3×10^6.

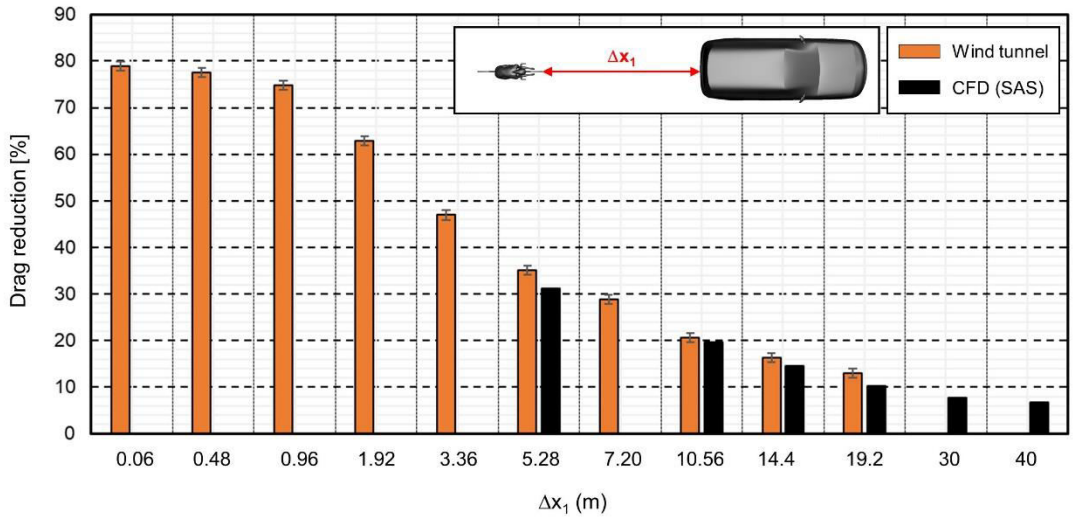

Fig. 7. Results of wind tunnel tests and CFD simulations: drag reduction for cyclist by drafting behind a car for different separation distances Δx_1.

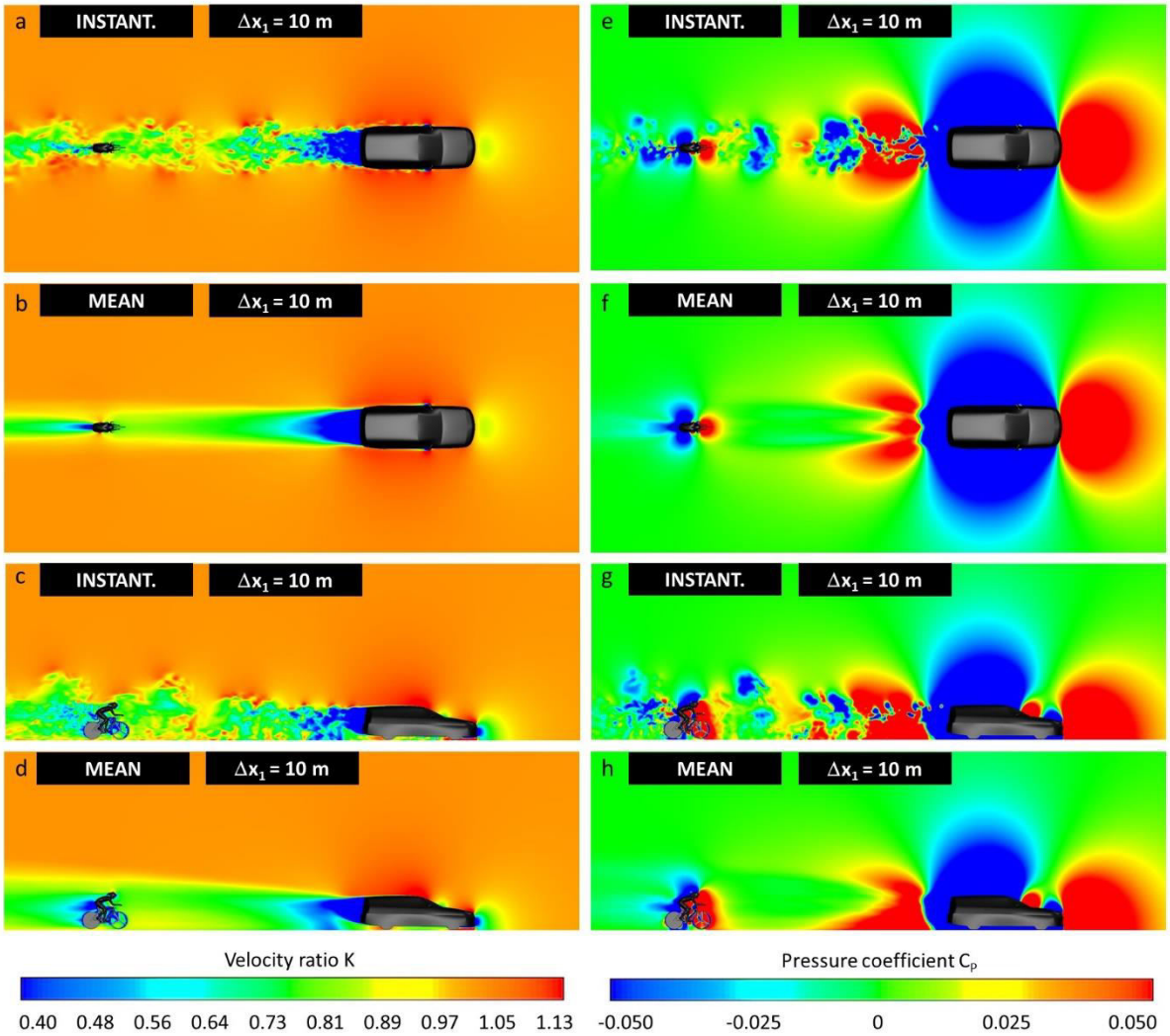

Fig. 8. Results of CFD simulations: (a-d) Contours of instantaneous and mean velocity ratio K in horizontal plane at 1 m height and in vertical centre plane for separation distance Δx_1 = 10 m. (e-h) Same for instantaneous and mean pressure coefficient C_P.

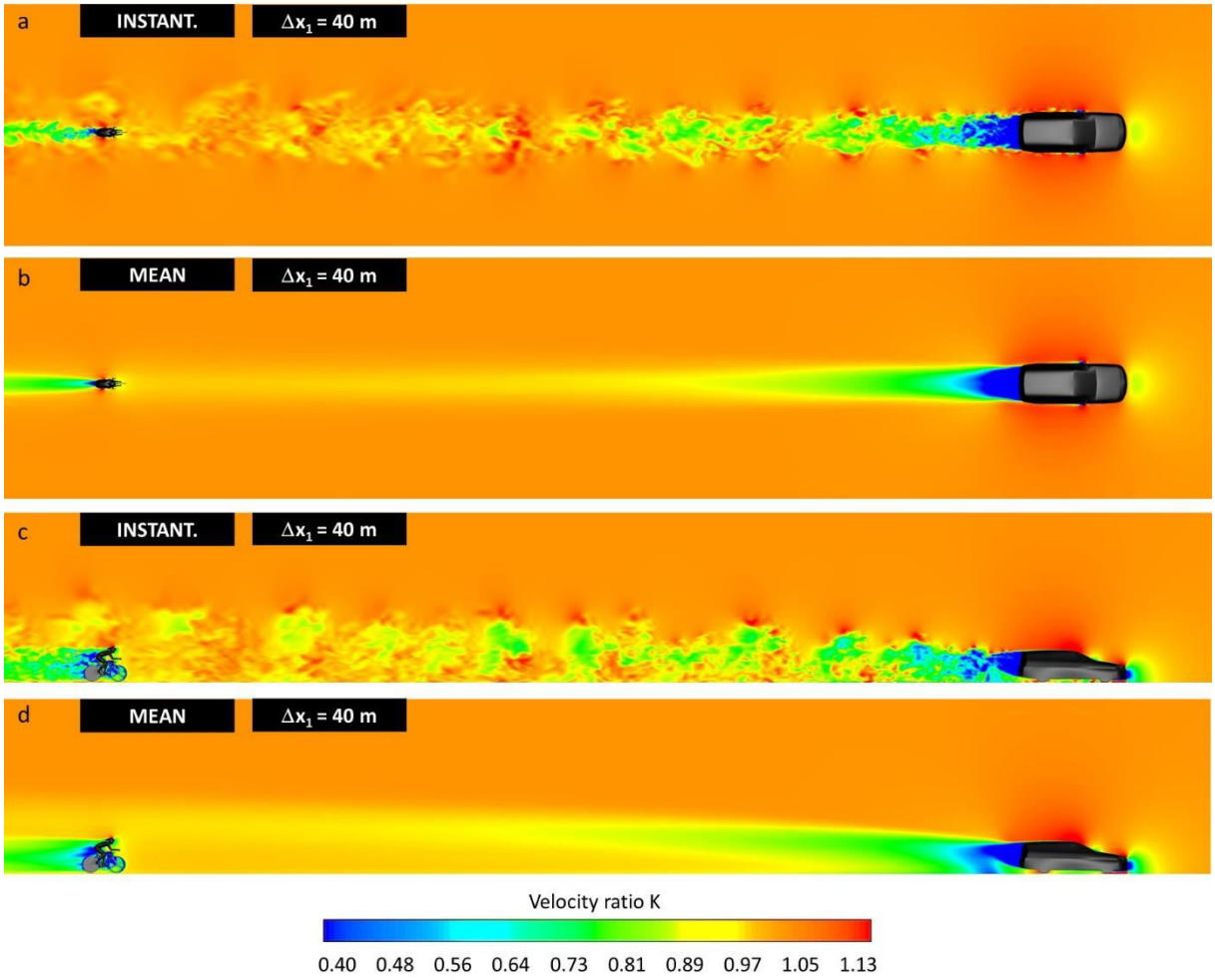

Fig. 9. Results of CFD simulations: Contours of instantaneous and mean velocity ratio K in horizontal plane at 1 m height and in vertical centre plane for separation distance $\Delta x_1 = 40$ m.

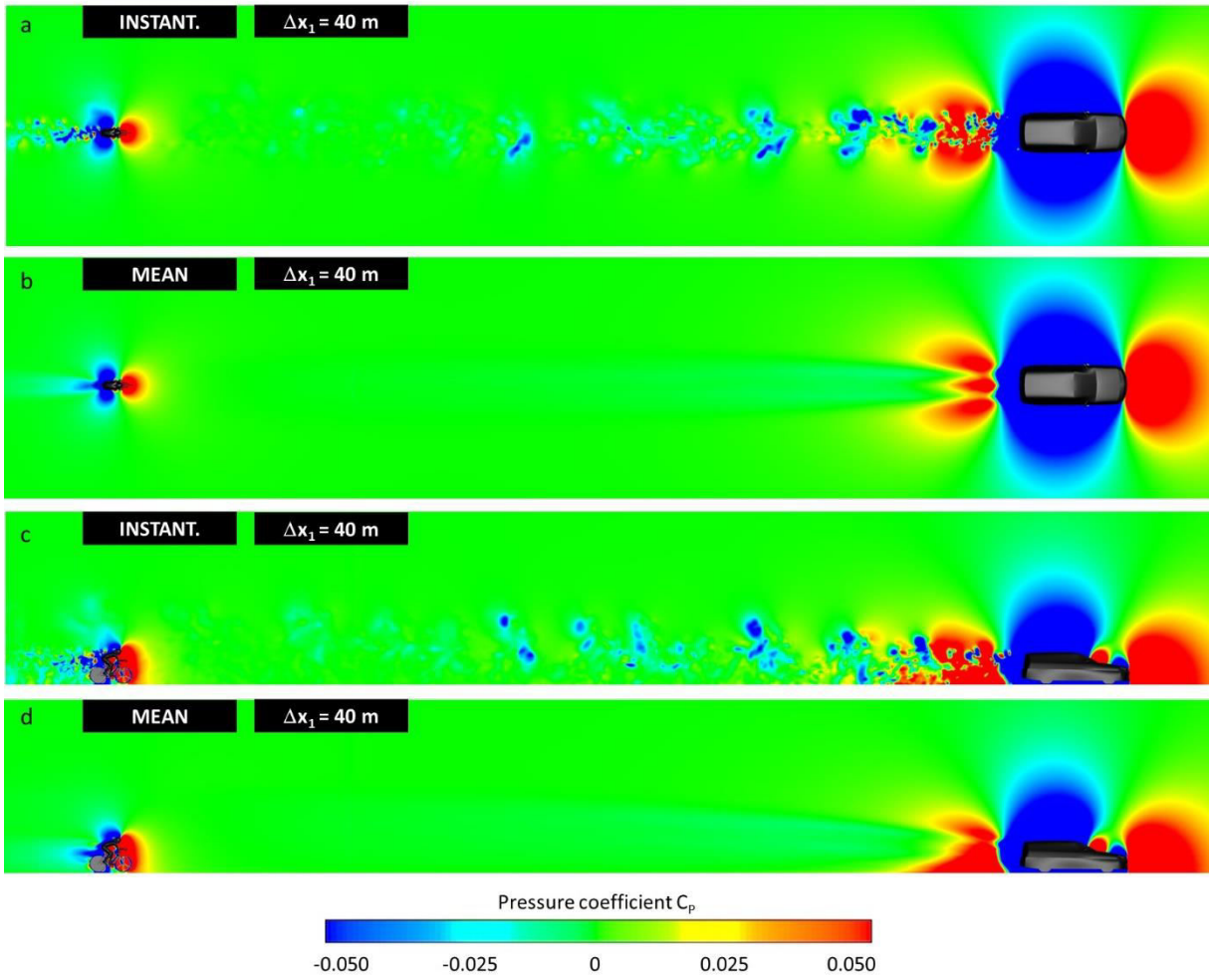

Fig. 10. Results of CFD simulations: Contours of instantaneous and mean pressure coefficient C_P in horizontal plane at 1 m height and in vertical centre plane for separation distance $\Delta x_1 = 40$ m.

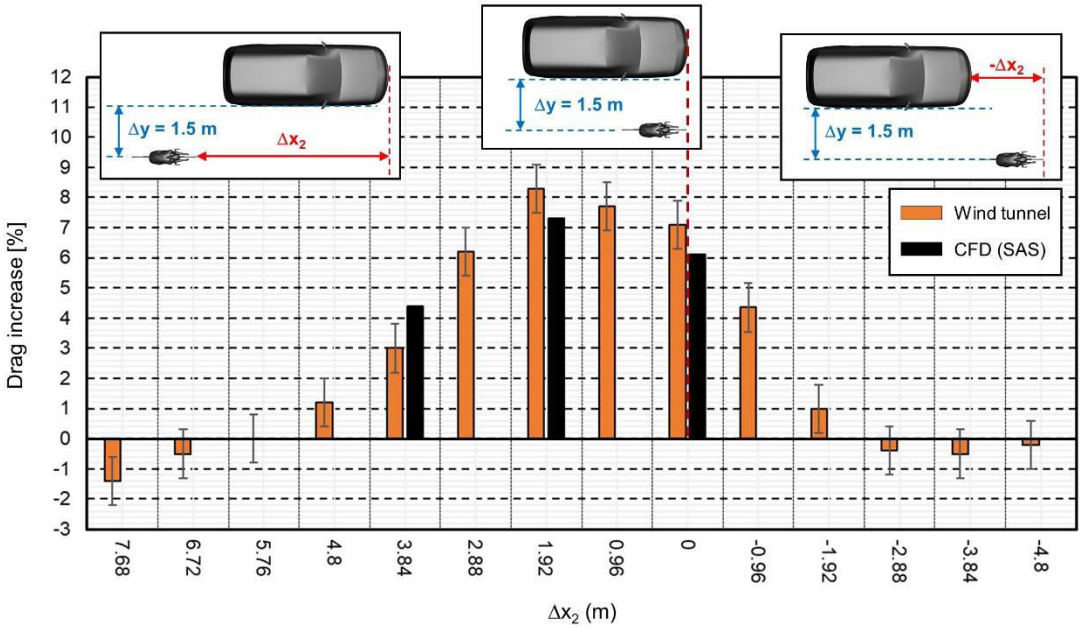

Fig. 11. Results of wind tunnel tests and CFD simulations: drag increase for cyclist riding nearby a car in staggered position for different streamwise separation distances Δx_2 and lateral distance $\Delta y = 1.5$ m.

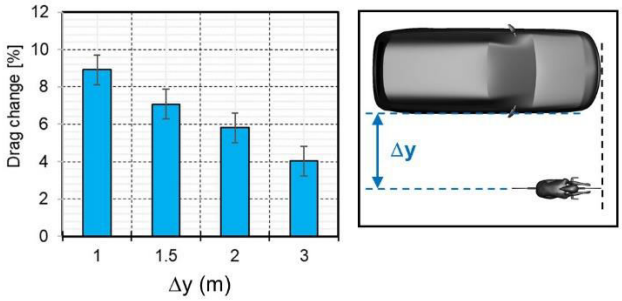

Fig. 12. Results of wind tunnel tests: drag change for cyclist riding next to a car with streamwise separation distance $\Delta x_2 = 0$ and different lateral distances Δy.

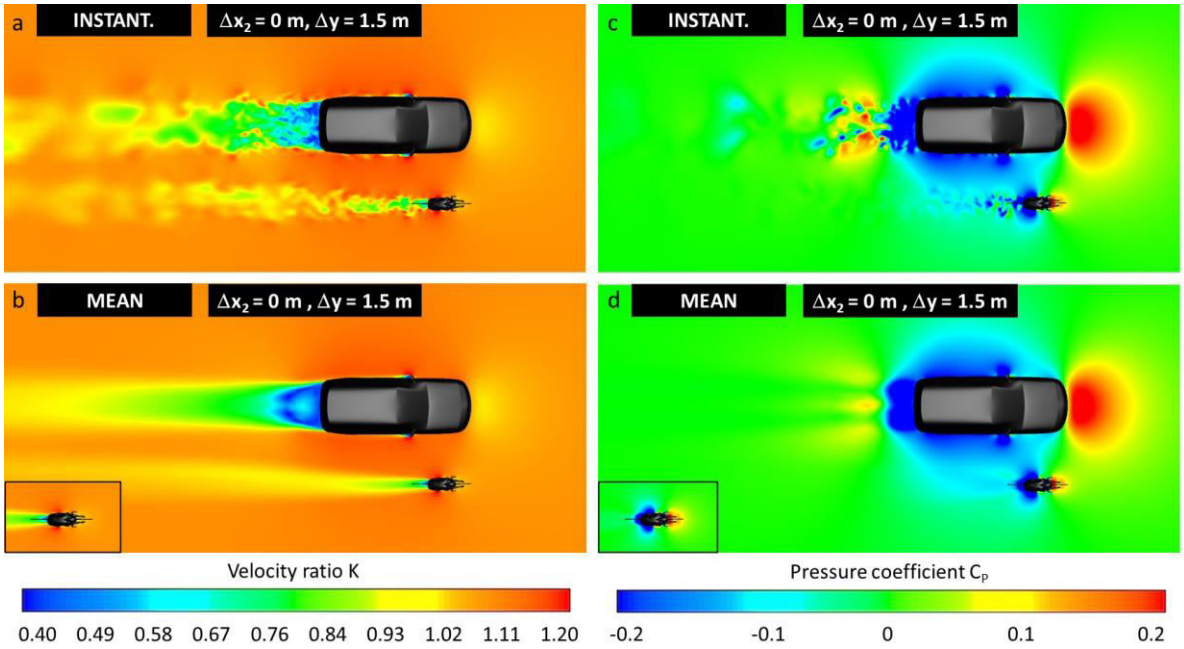

Fig. 13. Results of CFD simulations: Contours of instantaneous and mean velocity ratio K and pressure coefficient C_P in horizontal plane at 1 m height for cyclist next to car with $\Delta x_2 = 0$ and $\Delta y = 1.5$ m. Insert figure at bottom left is result for cyclist riding alone (reference situation).

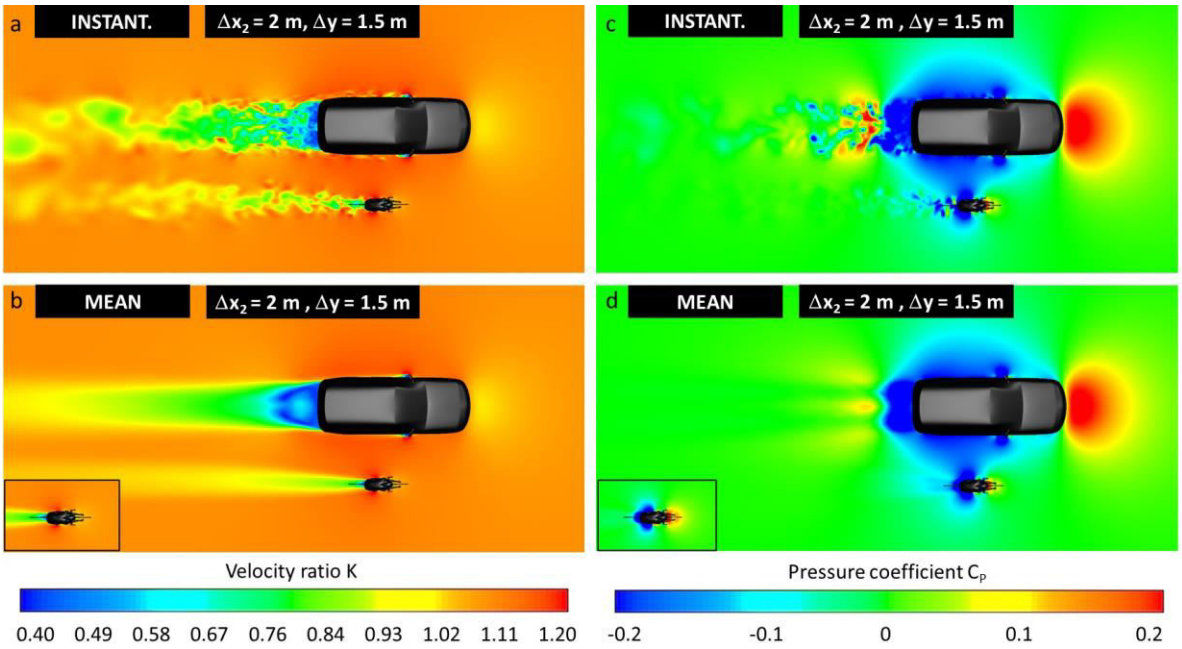

Fig. 14. Results of CFD simulations: Contours of instantaneous and mean velocity ratio K and pressure coefficient C_P in horizontal plane at 1 m height for cyclist next to car with Δx_2 = 2 m and Δy = 1.5 m. Insert figure at bottom left is result for cyclist riding alone (reference situation).

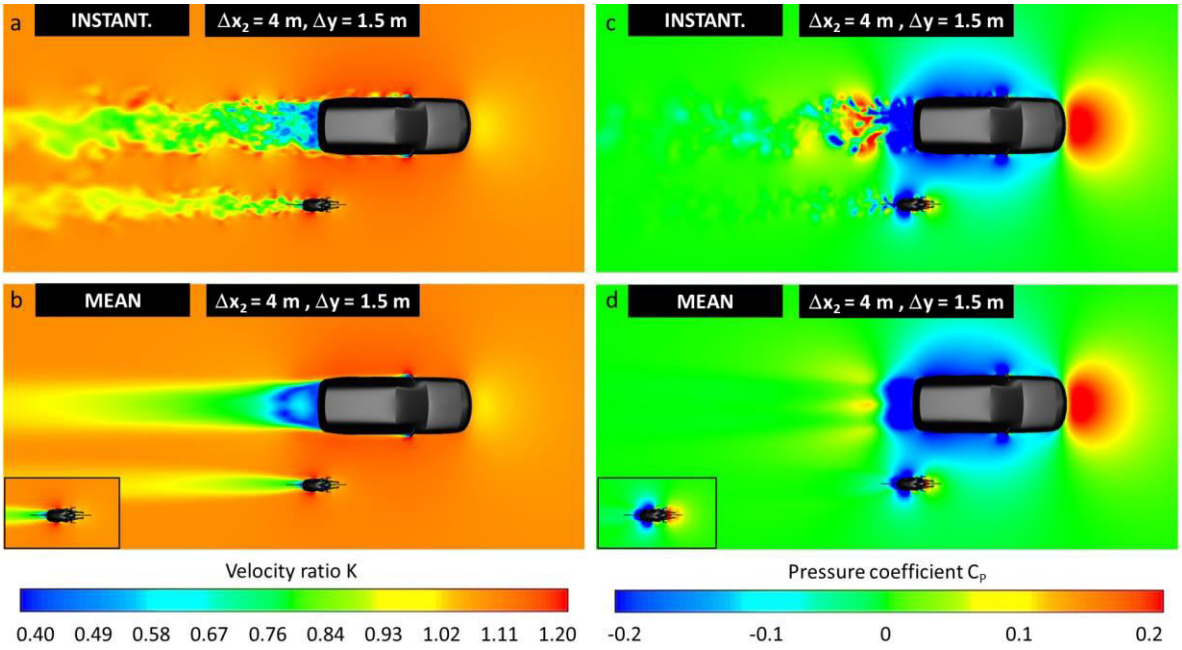

Fig. 15. Results of CFD simulations: Contours of instantaneous and mean velocity ratio K and pressure coefficient C_P in horizontal plane at 1 m height for cyclist next to car with Δx_2 = 4 m and Δy = 1.5 m. Insert figure at bottom left is result for cyclist riding alone (reference situation).

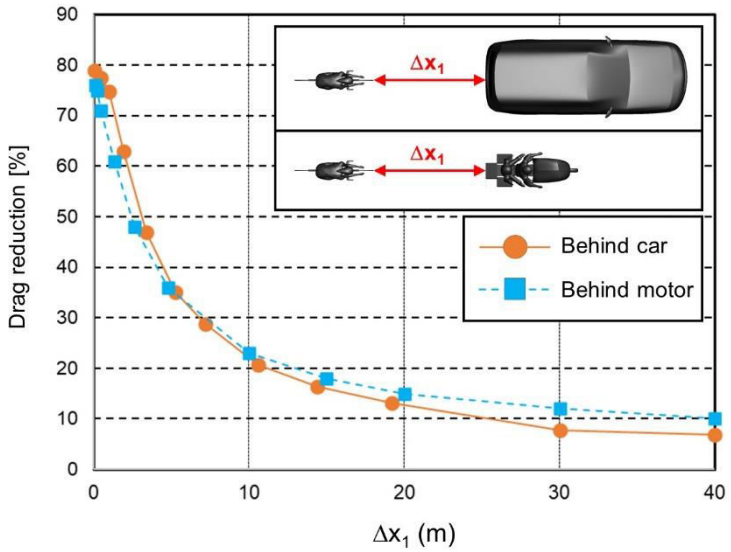

Fig. 16. Drag reduction for a cyclist drafting behind a car versus behind a motorcycle for different separation distances Δx_1.

Table 1: Drag reduction and potential speed increases and time gains for a cyclist drafting behind a car as a function of separation distance Δx_1, with reference to a cyclist riding alone at 13 m/s. Cycling power is kept constant.

Δx_1 (m)	Drag reduction (%)	Velocity (m/s)	Time gain per km (s)	Time gain per min (s)
0.06	79	33.8	47.3	36.9
0.48	78	33.0	46.6	36.3
0.96	75	30.7	44.3	34.6
1.92	63	24.3	35.8	27.9
3.36	47	19.5	25.6	20.0
5.28	35	17.1	18.6	14.5
7.20	29	16.2	15.2	11.8
10.56	21	15.1	10.6	8.2
14.4	16	14.5	8.2	6.4
19.2	13	14.2	6.6	5.2
30	8	13.7	4.0	3.1
40	7	13.6	3.5	2.7

Table 2: Drag increase and potential speed changes and time gains for a cyclist drafting behind a car as a function of streamwise separation distance Δx_2 and lateral separation distance Δy, with reference to a cyclist riding alone at 13 m/s. Cycling power is kept constant.

Δx_2 (m)	Δy (m)	Drag increase (%)	Velocity (m/s)	Time gain per km (s)	Time gain per min (s)
7.68	1.5	-1.4	13.12	0.7	0.5
6.72	1.5	-0.5	13.04	0.2	0.2
5.76	1.5	0.0	13.00	0.0	0.0
4.80	1.5	1.2	12.90	-0.6	-0.5
3.84	1.5	3.0	12.75	-1.5	-1.2
2.88	1.5	6.2	12.50	-3.1	-2.4
1.92	1.5	8.3	12.35	-4.1	-3.2
0.96	1.5	7.7	12.39	-3.8	-2.9
0	1.5	7.1	12.44	-3.5	-2.7
-0.96	1.5	4.4	12.65	-2.1	-1.7
-1.92	1.5	1.0	12.92	-0.5	-0.4
-2.88	1.5	-0.4	13.03	0.2	0.2
-3.84	1.5	-0.5	13.04	0.2	0.2
-4.80	1.5	-0.2	13.02	0.1	0.1
0	1	8.8	12.31	-4.3	-3.4
0	2	5.9	12.53	-2.9	-2.3
0	3	4.0	12.67	-2.0	-1.5